Gas phase synthesis and reactivity of dimethylaurate†

Nicole J. Rijs,[a,b,c] Gustavo B. Sanvido,[a,b,c,d] George N. Khairallah[a,b,c] and Richard A. J. O'Hair*[a,b,c]

Received 20th May 2010, Accepted 15th July 2010
DOI: 10.1039/c0dt00508h

A combination of multistage mass spectrometry experiments and DFT calculations were used to examine the synthesis and reactivity of dimethylaurate. Collision induced dissociation (CID) of $[(CH_3CO_2)_4Au]^-$ proceeded *via* reductive elimination of acetylperoxide to yield the diacetate $[CH_3CO_2AuO_2CCH_3]^-$, which in turn underwent sequential CID decarboxylation reactions to yield the organoaurates $[CH_3CO_2AuCH_3]^-$ and $[CH_3AuCH_3]^-$. The unimolecular chemistry of the dimethylaurate proceeds *via* a combination of bond homolysis to yield the methyl aurate radical anion $[CH_3Au]^{\bullet -}$ as well as formation of the gold dihydride $[HAuH]^-$. DFT calculations reveal that the latter anion is formed *via* a 1,2-dyotropic rearrangement to yield the isomer $[CH_3CH_2AuH]^-$, followed by a β-hydride elimination reaction. Ion-molecule reactions of $[CH_3AuCH_3]^-$ with methyl iodide did not yield any products even at relatively high concentrations of the neutral substrate and longer reaction times, indicating a reaction efficiency of less than 1 in 20 000 collisions. DFT calculations were carried out on two different potential energy surfaces (PES) for the reaction of $[CH_3AuCH_3]^-$ with CH_3I: (i) an S_N2 mechanism proceeding *via* a side-on transition state; and (ii) a stepwise mechanism proceeding *via* oxidative addition followed by reductive elimination. Both pathways have significant endothermic barriers, consistent with the lack of C–C bond coupling products being formed in the experiments. Finally, the reactivity of $[CH_3AuCH_3]^-$ is compared to the previously studied $[CH_3AgCH_3]^-$ and $[CH_3CuCH_3]^-$, as well as condensed phase studies on dimethylaurate salts.

Introduction

Metal mediated decarboxylation reactions, first studied by Pesci over a century ago,[1] and extensively examined for perfluorocarboxylates[2] are enjoying a renaissance.[3] Two main avenues of investigation are currently being pursued: (i) developing catalytic reactions for applications in organic synthesis;[4,5] and (ii) gas-phase mechanistic studies in which the decarboxylation reaction and the subsequent reactivity of the organometallic product are examined using multistage mass spectrometry approaches coupled with DFT calculations.[6,7] Examples of the former include protodecarboxylation reactions [4] and cross-coupling reactions,[5] while examples of the latter include our studies on the synthesis and reactivity of organocuprates and organoargentates.[8] The parent dimethylcuprate and dimethylargentate have been formed *via* double decarboxylation.[8a–d] Low energy collision induced dissociation (CID) on the metal acetates, $[CH_3CO_2MO_2CCH_3]^-$ (M = Cu, Ag), is dominated by CO_2 loss (eqn (1)), with acetate loss not occurring to any appreciable extent (eqn (2)). In the second CID step, the organometallates $[CH_3CO_2MCH_3]^-$ mainly undergo a second loss of CO_2 (eqn (3)), although some minor acetate loss was observed (eqn (4)). The methyl anion loss (eqn (5)), which could not be observed due to the low mass cut off of the instrument, was predicted by DFT calculations to be a high energy process.

$$[CH_3CO_2MO_2CCH_3]^- \rightarrow [CH_3CO_2MCH_3]^- + CO_2 \quad (1)$$

$$\rightarrow CH_3CO_2^- + MO_2CCH_3 \quad (2)$$

$$[CH_3CO_2MCH_3]^- \rightarrow [CH_3MCH_3]^- + CO_2 \quad (3)$$

$$\rightarrow CH_3CO_2^- + CH_3M \quad (4)$$

$$\rightarrow CH_3^- + CH_3CO_2M \quad (5)$$

The resultant dimethylmetallates undergo contrasting unimolecular [8e] and bimolecular reactivity.[8b] Thus, while dimethylargentate only fragments *via* bond homolysis (eqn (6)), dimethylcuprate undergoes both bond homolysis (eqn (6)) and a novel 1,2 dyotropic rearrangement [9] in which ethylcuprate is formed (eqn (8)) and subsequently fragments *via* β-hydride cleavage (eqn (9)).[8e] With regards to bimolecular reactivity, dimethylcurpate undergoes C–C bond coupling reactions with methyl iodide (eqn (10) and (11)), whereas dimethylargentate is unreactive.[8b] *Ab initio* calculations were carried out on the mechanisms of C–C bond coupling, which can potentially occur *via* two pathways (Scheme 1). These calculations were consistent with the experimental reactivity order and revealed that the dimethylcuprate prefers to react *via* an oxidative coupling (T-shaped transition state, Path B of Scheme 1) rather than an S_N2 mechanism (side-on transition state, Path A of Scheme 1).[8b]

[a]*School of Chemistry, The University of Melbourne, Victoria, 3010, Australia. E-mail: rohair@unimelb.edu.au; Fax: +61 3 9347 5180; Tel: +61 3 8344 2452*
[b]*Bio21 Institute of Molecular Science and Biotechnology, The University of Melbourne, Victoria, 3010, Australia*
[c]*ARC Centre of Excellence for Free Radical Chemistry and Biotechnology, Australia*
[d]*ThoMSon Mass Spectrometry Laboratory, Institute of Chemistry, State University of Campinas, 13083-970, Campinas, SP, Brazil*
† Electronic supplementary information (ESI) available: Further characterisation details. See DOI: 10.1039/c0dt00508h

$$[CH_3MCH_3]^- \rightarrow [CH_3M]^{\bullet -} + CH_3^{\bullet} \quad (6)$$

$$\rightarrow CH_3^- + [CH_3M] \quad (7)$$

$$\rightarrow [CH_3CH_2MH]^- \quad (8)$$

$$[CH_3CH_2MH]^- \rightarrow [HMH]^- + CH_2{=}CH_2 \quad (9)$$

$$[CH_3MCH_3]^- + CH_3I \rightarrow [CH_3MI]^- + CH_3CH_3 \quad (10)$$

$$\rightarrow I^- + CH_3CH_3 + CH_3M \quad (11)$$

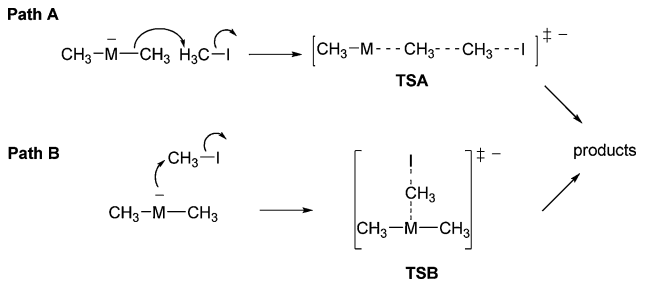

Scheme 1 Two mechanisms for C–C bond coupling of dialkylmetallates with methyl iodide: Path A follows a side on S_N2 mechanism *via* the transition state **TSA**; Path B proceeds *via* a T shaped transition state **TSB**.

Previously, dimethylaurate $[CH_3AuCH_3]^-$ has been synthesized in solution,[10] and its structure determined *via* X-ray crystallography.[11] Its condensed phase reactivity has also been examined [12] and several theoretical studies have been carried out.[13] Whereas, the gas phase reactions of the gold anion with methyl iodide have been found to proceed *via* an S_N2 reaction (eqn (12)),[14] until now, the gas phase synthesis and reactivity of $[CH_3AuCH_3]^-$ have not been examined.[15] The main reason has been that suitable precursor anions for decarboxylation (eqn (1) and (3)) have remained elusive. Here we report that electrospray ionisation of gold(III) acetate yields $[(CH_3CO_2)_4Au]^-$, which is a key precursor anion for the formation of $[CH_3AuCH_3]^-$. We also examine the gas phase unimolecular fragmentation reactions of $[CH_3AuCH_3]^-$ and its bimolecular ion-molecule reactions with methyl iodide.

$$Au^- + CH_3I \rightarrow I^- + CH_3Au \quad (12)$$

Experimental section

Reagents

Gold(III) acetate was obtained from Alfa Aesar. Methyl iodide was obtained from Aldrich. d_4-Acetic acid was obtained from Isotec. All chemicals were used without further purification.

Mass spectrometry

The CID mass spectra were recorded using a Finnigan LTQ FT hybrid linear ion trap (Finnigan, Bremen, Germany) fitted with the standard factory Finnigan electrospray ionization (ESI) source, as described previously.[16] Gold(III) acetate was dissolved in water (or alternatively, a 50/50 MeOH/H_2O mixture for longer solution phase stability of the required precursor ion) with a typical concentration of 1 mM. This solution was transferred to the electrospray source *via* a syringe pump at a rate of 5 μl min^{-1}. Typical electrospray source conditions with needle potentials of 2.5–3.0 kV and a heated capillary temperature of 250 °C and an activation Q (*i.e.*; the value that assigns the RF amplitude and frequency used to determine the motion of the ion in the trap) of 0.18–0.35 for a period of 30–100 ms were used. The desired precursor ion was mass selected and subjected to CID using standard isolation and excitation procedures. The anions were mass selected with a window of 1 Dalton to avoid complications arising from adjacent ^{13}C isotopes. Due to the low mass cut off of the ion trap, it can be a challenge to observe low mass ions when CID is carried out on a precursor ion. For example, we cannot observe the formation of the acetate anion at m/z 59 from CID on $[CH_3CO_2AuCH_3]^-$ (m/z 271) using the standard Q = 0.25. To check for possible formation of the acetate anion from $[CH_3CO_2AuCH_3]^-$, we have: (i) varied the value of Q to allow ions down to m/z 50 to be observed. Under these conditions, no acetate was observed; (ii) compared the total ion intensity of the trapped precursor ion *versus* the sum of the intensities of the precursor and all the CID product ions for a range of Q values (Table S11, ESI†). Since the ion signal loss is minimal upon CID and assuming that mass discrimination effects are absent, this suggests that acetate loss either does not occur, or is at best a very minor channel.

Ion-molecule reactions were performed on a modified Finnigan LCQ quadrupole ion trap mass spectrometer equipped with a Finnigan ESI source, as described previously.[17] The same solution of gold(III) acetate previously described was used and was injected with a flow of 5 μL min^{-1}. Typical electrospray source conditions involved needle potentials of 2.5–3.0 kV and heated capillary temperatures of 160–180 °C. Mass selection, collisional activation and ion-molecule reactions were carried out using the 'advanced scan' function of the LCQ software, which allows the Q value and the reaction time to be varied. The neutral substrate, methyl iodide, was introduced into the ion trap *via* the ion-molecule line at a concentration of *ca.* 2.5×10^{10} molecules per cm^3.

DFT calculations

Theoretical calculations were carried out to provide insights into the formation, unimolecular and bimolecular reactivity of the dimethylaurate anion (For reviews on theoretical calculation of gold systems see ref. 18). Gaussian 03 [19] utilizing the B3LYP hybrid functional[20] was used for all geometry optimizations and vibrational frequency calculations. The Stuttgart Dresden (SDD) basis set and effective core potential were used for the gold and iodine atoms while the 6–31+G(d) all electron basis set was used for carbon, oxygen and hydrogen.[21]

This combination was chosen: (i) to allow direct comparison with our previous work;[8c,d,f] (ii) as they are less computationally demanding than the higher levels of *ab initio* theory. Optimised B3LYP geometries of the dimethylaurate anionic complex were compared with those determined from X-ray crystallography.[11] There was excellent structural agreement between the calculated geometries and those determined experimentally (S9, ESI†).

Method comparison between B3LYP and MP2 with double and triple zeta basis sets on the hydrocarbon ligands was conducted (S10, ESI†). B3LYP was found to underestimate relative bond dissociation energies (BDEs) compared to MP2 methods (S10a–c, ESI†). This did not alter predicted reactive pathways in closed shell reactions. Choice between a double and triple zeta basis set was found to play a minor role, only improving the homolytic BDE with MP2, while the homolytic BDE was virtually the same when calculated with B3LYP/SDD6–31+G(d) *versus* B3LYP/SDD6–311++G(2d,p). Basis set superposition error was not corrected for, as weak ion neutral complexes were not pertinent to understanding reactive pathways. All transition state geometries were characterized by the presence of a single imaginary frequency and intrinsic reaction coordinates (IRC) were carried out to ensure smooth connection of reactants and products. All quoted energies include zero point vibrational energy.

Results and discussion

(1) Gas phase formation of dimethylaurate

Electrospray ionisation of gold(III) acetate in the negative ion mode results in several gold containing anions (Fig. S1, ESI†) of the type $[(CH_3CO_2)_{4-(x+y)}Au(OH)_x(O_2CCH_3)_y]^-$ (where $x + y = 0$–4). Collision induced dissociation (CID) of the gold(III) tetraacetate, $[(CH_3CO_2)_4Au]^-$ (*m*/*z* 433), results in reductive elimination of acetyl peroxide $(CH_3CO_2)_2$ to yield the desired gold(I) acetate anion, $[CH_3CO_2AuO_2CCH_3]^-$ (*m*/*z* 315), **1** as the only ionic product (eqn (13), Fig. S2a, ESI†). Due to the low mass cut-off of the ion trap, the loss of acetate anion (eqn (14)) is not observed.

$$[(CH_3CO_2)_4Au]^- \rightarrow [CH_3CO_2AuO_2CCH_3]^- + (CH_3CO_2)_2 \quad (13)$$

$$\rightarrow CH_3CO_2^- + (CH_3CO_2)_3Au \quad (14)$$

The CID MS^3 spectrum of $[CH_3CO_2AuO_2CCH_3]^-$, **1** (Fig. S2b, ESI†), highlights that decarboxylation proceeds cleanly (eqn (1)). This is consistent with previous low energy CID experiments performed on the related copper[8c] and silver[8d] acetates. An examination of the collision induced dissociation (CID) MS^4 spectrum of $[CH_3CO_2AuCH_3]^-$ (*m*/*z* 271), **3** (Fig. S2c, ESI†) reveals the presence of the sole loss of CO_2 to form $[CH_3AuCH_3]^-$ (*m*/*z* 227), **6** (eqn (3)). The ease of the second decarboxylation reaction is also consistent with the CID spectra of $[CH_3CO_2CuCH_3]^-$ [8c] and $[CH_3CO_2AgCH_3]^-$.[8d]

DFT calculations provide insight into the mechanistic pathways of the gold(III) tertraacetate decomposition. These results show that the reductive elimination pathway (eqn (13)) is endothermic by 1.62 eV, whereas acetate ligand dissociation (eqn (14)) is endothermic by 2.27 eV (Fig. S3, ESI†). Thus thermochemically, the reductive elimination of $(CH_3CO_2)_2$ to form the desired diacetate gold(I) precursor **1** is more likely to occur than the loss of an acetate anion.

The DFT energies for the decomposition of $[CH_3CO_2AuO_2CCH_3]^-$, **1**, and $[CH_3CO_2AuCH_3]^-$, **3**, are shown in Fig. 1a and 1b. The activation energy required for decarboxylation of $[CH_3CO_2AuO_2CCH_3]^-$ (Fig. 1a, **TS1-2**, 1.80 eV, eqn (1)) is much lower than the energy required for loss of the acetate ligand (Fig. 1a, 2.91 eV, eqn (2)), suggesting that decarboxylation will be overwhelmingly favoured in this step. Fig. 1b reveals that the energy required for loss of the acetate ligand is significantly lowered (1.72 eV, eqn (4)), but is still nearly 0.1 eV above the activation energy for decarboxylation of **3** (**TS3-5**, 1.65 eV, eqn (3)). Thus decarboxylation is expected to be the preferred path under low energy CID conditions. The optimised decarboxylation transition state geometries (Fig. 1, **TS1-2** and **TS3-5**) are 3 centred in both cases, similar to their copper and silver analogues.[8c,d] Therefore, the small calculated energy difference in conjunction with the calculated tight transition state (**TS3-5**), suggest that both pathways might occur. As noted in the experimental section, additional experiments were carried out to establish whether acetate loss may be a hidden channel for $[CH_3CO_2AuCH_3]^-$. These results suggest that acetate loss either does not occur, or is at best a very minor channel. Thus the decarboxylation reactions, which are predicted to be the lowest energy pathways for both $[CH_3CO_2AuO_2CCH_3]^-$, **1**, and $[CH_3CO_2AuCH_3]^-$, **3**, appear to be the only pathways that operate under the low energy CID conditions of the ion trap (Fig. S2, ESI†).

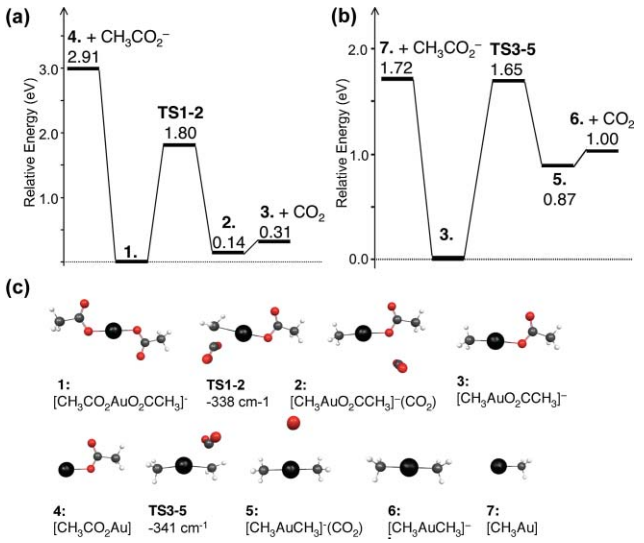

Fig. 1 B3LYP/SDD6-31+G(d) calculated energies for minima and transition states relevant to fragmentation of: **(a)** $[CH_3CO_2AuO_2CCH_3]^-$ *via* decarboxylation (right hand side) and acetate loss (left hand side); **(b)** $[CH_3CO_2AuCH_3]^-$ *via* decarboxylation (right hand side) and ligand loss (left hand side); **(c)** structures of minima and transition states relevant to the reductive elimination and first and second decarboxylation pathways. The cartesian coordinates of all structures are given in Supplementary Figures S3 and S4†.

(2) Gas phase fragmentation reactions of dimethylaurate

Dimethyl aurate salts decompose in the condensed phase *via* formation of ethane, although the mechanism of this thermal decomposition has yet to be determined.[13b] Thus, we have examined the fragmentation reactions of mass selected dimethylaurate, formed as described above (*via* the sequence of CID reactions: eqn (13) → eqn (1) → eqn (3)). Low energy CID of $[CH_3AuCH_3]^-$, *m*/*z* 227, results in the MS^5 spectrum shown in Fig. 2a. In addition, the CID reactions of the following deuterium isotopologues were examined: $[CD_3AuCD_3]^-$ (Fig. 2b), *m*/*z* 233; and $[CD_3AuCH_3]^-$ (Fig. 2c), *m*/*z* 230. An examination of the CID spectra in Fig. 2

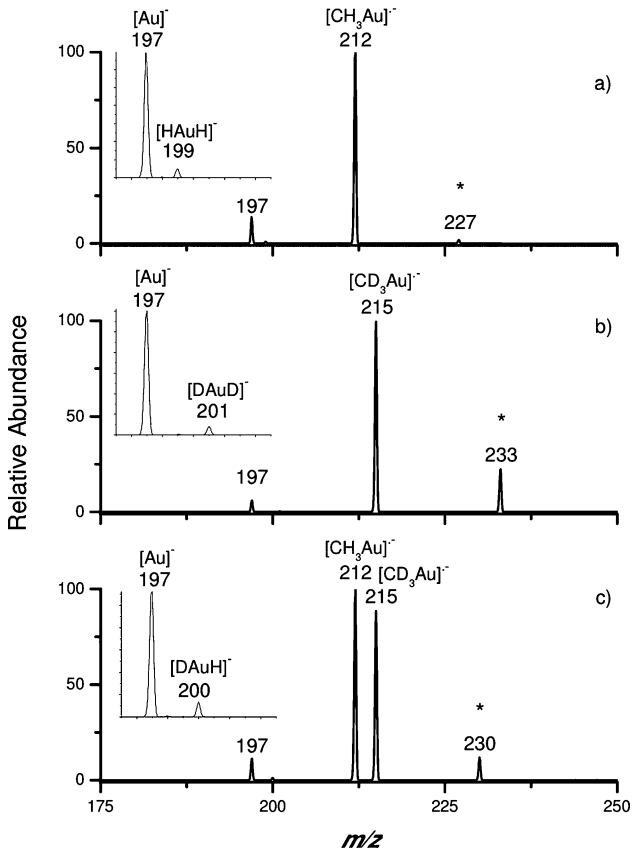

Fig. 2 Mass spectra showing CID of dimethylaurates: **(a)** $[CH_3AuCH_3]^-$, *m/z* 227; **(b)** $[CD_3AuCD_3]^-$, *m/z* 233; **(c)** $[CH_3AuCD_3]^-$, *m/z* 230. The mass selected precursor ion is marked with an *.

reveals that the major fragmentation pathway for dimethylaurate is bond homolysis (eqn (6)), yielding the hitherto unknown radical anion $[CH_3Au]^{\bullet-}$, which is related to the previously described radical anions $[CH_3Cu]^{\bullet-}$, $[CH_3Ag]^{\bullet-}$, [8e,f] and $[PhAu]^{\bullet-}$.[22] This contrasts with the fragmentation reactions of $[CH_3CO_2AuCH_3]^-$, described above, which did not undergo bond homolysis. Due to the low mass cut off of the ion trap, we are unable to observe the bond heterolysis product, which would yield the methyl anion and the neutral methylgold (eqn (7)). The gold anion, Au^-, is formed most likely as a result of the secondary loss of methyl radical, as shown in eqn (15) and confirmed by an additional stage of CID on $[CH_3Au]^{\bullet-}$ (data not shown). The dihydride anion, $[HAuH]^-$, is also formed as an additional fragment ion (for previous studies on gold hydrides, see ref. 23). CID of the deuterium labelled ions $[CD_3AuCD_3]^-$ (Fig. 2b) and $[CD_3AuCH_3]^-$ (Fig. 2c) result in the specific formation of $[DAuD]^-$ and $[DAuH]^-$ respectively, consistent with a 1,2 dyotropic rearrangement reaction [9] (eqn (8)) followed by β-hydride transfer (eqn (9)). By directly comparing the abundances of $[CD_3Au]^{\bullet-}$ (formed by cleavage of the Au–CH_3 bond, eqn (16)) with that of $[CH_3Au]^{\bullet-}$ (formed by cleavage of the Au–CD_3 bond, eqn (17)) in the CID spectrum of $[CD_3AuCH_3]^-$, an inverse deuterium secondary kinetic isotope effect (k_H/k_D) for homolytic cleavage of the Au–C bond was determined to be 0.89. This value is in the same range as the homolytic cleavage of the Cu–C bond (k_H/k_D = 0.90) and homolytic cleavage of the Ag–C bond (k_H/k_D = 0.89).[8e]

$$[CH_3M]^{\bullet-} \rightarrow M^- + CH_3^{\bullet} \quad (15)$$

$$[CD_3MCH_3]^- \rightarrow [CD_3M]^{\bullet-} + CH_3^{\bullet} \quad (16)$$

$$\rightarrow [CH_3M]^{\bullet-} + CD_3^{\bullet} \quad (17)$$

The potential energy surface associated with the unimolecular decomposition of $[CH_3AuCH_3]^-$, **6**, is shown in Fig. 3. Three pathways are examined: bond homolysis (eqn (6)), bond heterolysis (eqn (7)), and the 1,2-dyotropic rearrangement followed by β-hydride elimination (eqn (8) and eqn (9)). The lowest energy pathway was found to be that of bond homolysis (Fig. 3a, 2.73 eV). This is consistent with the predicted homolytic BDE of previously calculated dimethyl metallates being the lowest calculated pathway.[8] Bond heterolysis is predicted to be a high-energy process. On the B3LYP surface, there is disagreement between experiment and theory with regards to the 1,2-dyotropic rearrangement, which is predicted to be *ca.* 0.70 eV higher in energy than bond homolysis and is thus not expected to be observed experimentally. It is known that DFT generally underestimates BDEs.[24] Thus, in our work on the related fragmentation reactions of $[CH_3CuCH_3]^-$, closer agreement between experiment and theory was observed for *ab initio* calculations carried out at the MP2/SDD6-311++G(2d,p) level of theory.[8e,f] This effect was due to both a slight lowering of the activation barrier of the rearrangement and an increase in homolytic BDE. We have assessed this effect on the current gold system and the same trend was observed (S10c, black line, ESI†). Thus an increase in homolytic BDE and slight decrease in activation barrier is observed, leading to a difference of only 0.05 eV. At this level of theory, the 1,2-dyotropic rearrangement reaction is predicted to occur. Finally, attempts to locate a triplet transition state for the 1,2-dyotropic rearrangement failed and yielded the complex $CH_3AuCH_2(H)^-$ instead. Since this complex is also much higher in energy than the singlet state, spin crossing is not expected to be an important factor in the observed reactivity (S5, ESI†).

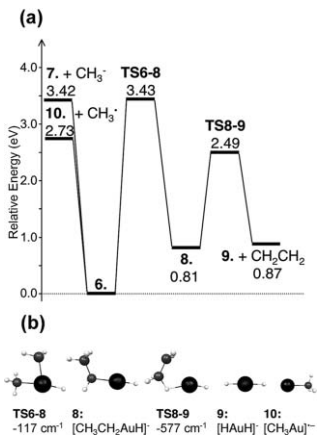

Fig. 3 B3LYP/SDD6-31+G(d) **(a)** calculated energies for fragmentation of $[CH_3AuCH_3]^-$; **(b)** structures of both minima and transition states relevant to the isomerization to $[CH_3CH_2MH]^-$ (eqn (8)) and fragmentation *via* β-hydride elimination (eqn (9)). The cartesian coordinates of all structures are given in Supplementary Figure S5†.

(3) Gas phase ion-molecule reactions of dimethylaurate with methyl iodide

Kochi *et al.*[12c] have established that dimethyl aurate salts react with methyl iodide *via* oxidative addition to form organogold(III) species, which are either stable (eqn (18)) or decompose generating ethane and metallic gold (eqn (19)) depending on the nature of the coordinating ligands (PPh_3 = triphenylphosphine; PMDT = *N*,*N*,*N*′,*N*′,*N*″-pentamethyldiethylenetriamine). In order to determine whether these reactions occur in the gas phase, we next subjected dimethylaurate to ion-molecule reactions with methyliodide. No reaction was observed, even at high concentrations of methyliodide (*ca.* 2.5×10^{10} molecules per cm^3), and at the longest possible reaction times (10 s). An estimate of the upper limit for reaction is *ca* 5×10^{-14} cm^3 $molecule^{-1}$ s^{-1}, corresponding to a reaction efficiency of less than 1 in 20 000 collisions.

$$(CH_3)_2Au^{I}Li[PPh_3] + CH_3I \rightarrow (CH_3)_3Au^{III}PPh_3 + LiI \quad (18)$$

$$2\,(CH_3)_2Au^{I}Li[PMDT] + 2\,CH_3I \rightarrow 2\,(CH_3)_3Au^{III} + 2\,Li[PMDT]I \rightarrow 3\,CH_3CH_3 + 2\,Au \quad (19)$$

In order to gain insight into the lack of reactivity of $[CH_3AuCH_3]^-$ towards CH_3I, we have carried out DFT calculations on the two potential mechanisms shown in Scheme 1. We note that previous theoretical calculations of the reactions of $[CH_3CuCH_3]^-$ and $[CH_3AgCH_3]^-$ with CH_3I have been carried out at the MP2/6-31++G(d,p) level of theory,[8b] while the reaction of $[CH_3CuCH_3]^-$ with methyl and vinyl chloride has also been studied at the B3LYP/6-31+G(d) level of theory.[25] Slight differences in the mechanisms of Path B were observed from these two studies. At the MP2 level, the reaction is a one step process proceeding *via* one transition state, while at the B3LYP level, reaction proceeds *via* two steps involving an oxidative addition transition state and a reductive elimination transition state. Thus, for consistency and to allow direct comparisons to be made, we have studied the reactions of all three coinage metal dimethylmetallates with CH_3I *via* Paths A and B (Scheme 1) at the B3LYP/SDD6-31+G(d) level of theory. The potential energy surfaces for these reactions are given in Fig. 4 for $[CH_3AuCH_3]^-$ and in Fig. S8† for $[CH_3CuCH_3]^-$ and $[CH_3AgCH_3]^-$, while key energies are compared for the three metallates in Table 1 and discussed in detail in section (4) below. Here we focus on a discussion of the potential reactions of $[CH_3AuCH_3]^-$ with CH_3I and why these do not appear to occur under our experimental conditions.

Three different sets of products are possible: (i) formation of $[CH_3AuI]^-$ and CH_3CH_3 (eqn (10)), which is predicted to be exothermic by 2.77 eV; (ii) formation of I^-, $[CH_3Au]$ and CH_3CH_3 (eqn (11)), which is predicted to be exothermic by 1.26 eV; (iii) formation of I^- and $[(CH_3)_3Au]$ (eqn (20)), which is predicted to be endothermic by 0.33 eV. The fact that $[CH_3AuI]^-$ and I^- are not observed in the experiments suggests that even though eqn (10) and eqn (11) are exothermic overall, the mechanisms for their formation *via* either pathways A or B of Scheme 1 must involve barriers. An examination of Fig. 4 reveals that this is indeed the case. The S_N2 mechanism (side-on transition state, Path A of Scheme 1) has a transition state (**TS14-13** of Fig. 4) that lies 0.2 eV above separated reactants and is thus not expected to give rise to I^-. The potential energy surface associated with Path B of Scheme 1

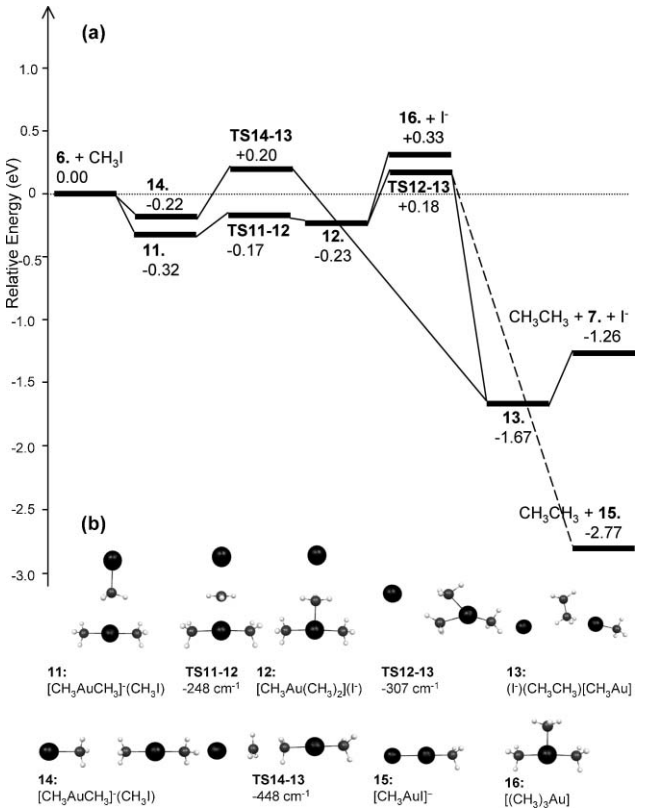

Fig. 4 B3LYP/SDD6-31+G(d) **(a)** calculated reaction energy profiles for Paths A and B of Scheme 1 for the reaction of $[CH_3AuCH_3]^-$ with CH_3I; **(b)** structures of both minima and transition states relevant to Paths A and B. The cartesian coordinates of all structures are given in Supplementary Figure S6†.

involves two transition states: the oxidative addition transition state (**TS11-12** of Fig. 4) that lies 0.17 eV below separated reactants and the reductive elimination transition state (**TS12-13** of Fig. 4) that lies 0.18 eV above separated reactants. Thus if intermediate **12** is formed, it can neither yield I^- *via* eqn (20) due to the overall endothermicity of 0.33 eV nor $[CH_3AuI]^-$ or I^- due to the barrier associated with **TS12-13**. Thus the only possible options for **12** are to dissociate back to reactants or to be collisionally stabilized *via* the helium bath gas. As we do not observe an adduct at *m*/*z* 369 in our experiments, we must assume that if **12** is transiently formed, it rapidly dissociates back to reactants.

$$[CH_3MCH_3]^- + CH_3I \rightarrow I^- + [(CH_3)_3M] \quad (20)$$

(4) Comparisons of reactivity trends in group 11 metallates

Since the gas phase chemistry of $[CH_3MCH_3]^-$ has been studied for M = Cu and Ag[8b,c,d,e] and now for M = Au (this work), we are able to compare trends in their formation and reactivity (Table 1). The DFT calculated pathways for the first and second decarboxylation steps (eqn (1) and (3)) to form $[CH_3MCH_3]^-$ have energies for the transition states for decarboxylation that are not only of a similar magnitude (compare eqn (1) and eqn (3) data in Table 1), but are also the lowest of all potentially competing pathways. Acetate loss (eqn (2) and eqn (4)) is always higher in energy, consistent with it being a minor or non-existent process in the low energy CID spectra of $[CH_3CO_2MO_2CCH_3]^-$

Table 1 Summary of DFT predicted energetics (in eV) for various coinage metal reactions

Anion	Type of reaction	M = Cu	M = Ag	M = Au
$[(CH_3CO_2)_2M]^-$	Decarboxylation (eqn (1))[a]	1.67	1.61	1.80
	Acetate loss (eqn (2))	2.68	2.30	2.91
$[CH_3CO_2MCH_3]^-$	Decarboxylation (eqn (3))[a]	1.67	1.66	1.65
	Acetate loss (eqn (4))	1.86	1.68	1.72
	Methyl anion loss (eqn (5))	4.36	4.05	5.33
$[CH_3MCH_3]^-$	Bond homolysis (eqn (6))	2.72	2.41	2.73
	Methyl anion loss (eqn (7))	3.19	3.03	3.42
	Dyotropic rearrangement (eqn (8))[a]	3.43	3.55	3.43
$[CH_3CH_2MH]^-$	β-hydride transfer (eqn (9))[a]	1.65 (2.03)[b]	1.83 (2.01)[b]	1.68 (2.49)[b]
$[CH_3MCH_3]^- + CH_3I$	$[CH_3MI]^- + CH_3CH_3$ (eqn (10))[c]	−3.05	−3.14	−2.77
	$I^- + CH_3CH_3 + CH_3M$ (eqn (11))[c]	−1.97	−1.66	−1.26
	$I^- + [(CH_3)_3M]$ (eqn (20))[c]	+0.07	+0.45	+0.33
	Side on S_N2 (Scheme 1, Path A)[d]	+0.02	+0.01	+0.20
	T shape oxidative addition (Scheme 1, Path B)[d]	−0.28	−0.13	−0.17
	T shape reductive elimination[d]	−0.20	+0.22	+0.18

[a] Activation energy for transition state relative to precursor ion. [b] Energy for transition state relative to $[CH_3MCH_3]$ [c] Reaction energy relative to separated reactants [d] Relative energy for transition state compared to separated reactants.

and $[CH_3CO_2MCH_3]^-$. The DFT predicted heterolytic bond dissociation energies for acetate loss from $[CH_3CO_2MO_2CCH_3]^-$ and $[CH_3CO_2MCH_3]^-$ show a decrease from copper to silver, and then an increase from silver to gold. This is consistent with several experimental and theoretical studies of the bond strengths of ligated group 11 coinage metals (eqn (21) and eqn (22), where M = Cu, Ag, Au). For example, a recent review by Roithová and Schröder[6] highlights the order Au > Cu > Ag in the BDE for eqn (21) where L = H_2O. Similar BDE trends were observed in a recent computational study on $[(H_3P)_2M]^+$ (eqn (21)) and $[ClMPH_3]$ (eqn (22)), where the relativistic effect of Au on these BDEs was highlighted.[12d]

$$[L_2M]^+ \rightarrow [LM]^+ + L \quad (21)$$

$$[ClMPH_3] \rightarrow [ClM] + PH_3 \quad (22)$$

The DFT calculations on the potential unimolecular fragmentation channels of the organometallates $[CH_3MCH_3]^-$ reveal that bond homolysis is the lowest energy pathway in all three cases, with M = Ag requiring the lowest energy. This is consistent with the low energy CID spectra, where the bond homolysis channel (eqn (6)) is the dominant fragmentation pathway in all cases. Methyl anion loss (eqn (7)) is theoretically predicted to be unfavourable for all metals. A key difference between the metals is that $[HMH]^-$ is experimentally observed as a minor product for M = Cu and Au, but is not observed when M = Ag. MP2/SDD6-311++G(2d,p) calculations have been shown to provide better predictions for the homolytic BDE for all metals.[8e] A comparison of these values reveals that the lack of $[HMH]^-$ in the case of silver is due to its much lower homolytic BDE with the difference in barrier compared to a 1,2-dyotropic rearrangement being 0.11 eV, 1.06 eV and 0.05 eV for M = Cu, Ag and Au respectively (Figure S10c†,[8e]). On a final note, the transition state energies for β-hydride transfer for $[CH_3CH_2MH]^-$ (eqn (9)) are similar for Cu and Au. Thus in future studies it will be interesting to see if β-hydride transfer reactions are important for a range of mixed aurates, $[CH_3AuR]^-$.

Only the organocuprate $[CH_3CuCH_3]^-$ is reactive towards methyl iodide. Formation of $[(CH_3)_3M]$ (eqn (20)) is predicted to be endothermic for all metals. Formation of the C–C bond coupled products are predicted to be exothermic for eqn (10) and eqn (11) for all metals. Thus the differences in observed reactivity of the dimethylmetallates arises from barriers associated with these reactions. For all metals, the side-on S_N2 pathway (Path A, Scheme 1, Fig. S8†) has transition states with energies that lie above the separated reactants, and is thus not expected to proceed under the near thermal rt conditions of the quadrupole ion trap.[26] The key transition state for the T-shaped pathway (Path B, Scheme 1) that determines whether C–C bond coupling products are observed is not the one associated with the oxidative addition, but rather the one associated with the reductive elimination. The potential energy surfaces clearly highlight that the TS for this step is only favoured in the case of Cu where the energy is 0.2 eV lower than the separated reactants, whereas, in the cases of Ag and Au, it is 0.22 and 0.18 eV above the separated reactants. This is consistent with the experiments, where only $[CH_3CuCH_3]^-$ gives products arising from C–C bond coupling.[8b]

The structures of the transition states associated with oxidative addition and reductive elimination warrant attention and are given in Fig. 5. An examination of their geometries reveals two interesting trends. Firstly, the oxidative addition transition state geometries (Fig. 5a–c) show a notable deviation from the linear metallate structure in the case of copper, whereas there is little change in the bond angle for the case of silver or gold. A previous study of inorganic coinage metal complexes has shown that gold prefers a dicoordinate structure; the reason being that the energy required for deformation of dicoordinate gold complexes is higher than that of silver or copper.[27] This is consistent with the result here, where gold resists in oxidative addition by having a higher deformation energy.

The deformation of a tricoordinate complex (pyramidalization) has also been shown to be higher in energy for gold complexes.[27] This phenomenon manifests itself in the geometries of the reductive elimination transition state structures shown in Fig. 5d–f. Whereas copper and silver, aided by the presence of an iodide anion, are able to deform to allow a reductive elimination through a transition state that is pyramidalized, the transition state geometry for gold is dramatically different, being Y-shaped

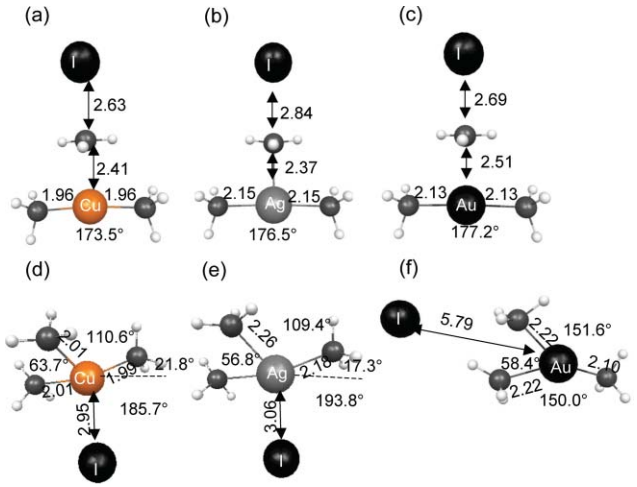

Fig. 5 DFT optimised key transition state geometries of C–C bond coupling of CH_3I with dimethylmetallates: **(a)** oxidative addition for $[CH_3CuCH_3]^-$; **(b)** oxidative addition for $[CH_3AgCH_3]^-$; **(c)** oxidative addition for $[CH_3AuCH_3]^-$; **(d)** reductive elimination for $[CH_3CuCH_3]^-$; **(e)** reductive elimination for $[CH_3AgCH_3]^-$; **(f)** reductive elimination for $[CH_3AuCH_3]^-$.

and planar. This geometry effect has also been noted previously by Nakamura and co-workers.[13c] Thus, in the gold case, the iodine is of little assistance, preferring to be part of an ion-molecule complex with hydrogen bonding (the distance of the iodide from the Au center is *ca.* 6 Å – see Fig. 5f), rather than coordinated to the metal as it is for both copper and silver (where the distance is *ca.* 3 Å in Fig. 5d and 5e).

Conclusions

Here we have extended the double decarboxylation strategy developed for copper and silver carboxylates[8] to the synthesis of dimethylaurate. This has rounded out the gas-phase reactivity studies of coinage metal dimethylmetallates, and a number of interesting trends have emerged. For example, the unimolecular chemistry of dimethylaurate is more similar to that of dimethylcuprate, where $[CH_3M]^{\bullet -}$ bond homolysis (eqn (6)) and $[HMH]^-$ (eqn (9)) (formed *via* the 1,2 dyotropic rearrangement (eqn (8)) and β-hydride elimination (eqn (9)) are experimentally observed. In contrast, dimethylcuprate is the only species that reacts with methyliodide *via* C–C bond coupling. This is consistent with DFT calculations that reveal the existence of barriers associated with the reductive elimination reactions for both dimethylargentate and dimethylaurate.

Studies on the formation and reactions of other organometallic ions are underway. Preliminary data suggest that a range of mixed aurates of the type $[CH_3AuR]^-$ can be formed *via* an analogous sequence of CID reactions to those described here (*cf*. eqn (13) → eqn (1) → eqn (3)) and that decarboxylation reactions can be extended to catalytically relevant palladium systems. The results of these studies will be presented in due course.

Acknowledgements

We thank the ARC for financial support *via* grant DP0558430 (to RAJO) and through the ARC CoE program. NJR thanks: (i) the Faculty of Science for a Science Faculty Scholarship; (ii) The University of Melbourne for a Postgraduate Overseas Research Experience Scholarship (PORES) to travel to the University of Tokyo; and (iii) Prof. Eiichi Nakamura of the University of Tokyo for hosting a visit to carry out theoretical studies on metal based systems. VPAC is acknowledged for the generous provision of computational resources. VICS is acknowledged for the Chemical Sciences High Performance Computing Facility. GBS thanks São Paulo Research Foundation – FAPESP for a scholarship and the University of Melbourne for providing an Occupational Traineeship.

References

1 L. Pesci, *Atti Accad. Naz. Lincei, Cl. Sci. Fis., Mat. Nat., Rend.*, 1901, **10**(I), 362–363. For an English abstract, see: L. Pesci, *J. Chem. Soc., Abstr.*, 1901, **80**, 576.
2 (*a*) G. B. Deacon, *Organomet. Chem. Rev., Sect. A*, 1970, **5**, 355; (*b*) G. B. Deacon, S. J. Faulks and G. N. Pain, *Adv. Organomet. Chem.*, 1986, **25**, 237–276.
3 (*a*) L. J. Gooßen, K. Gooßen, N. Rodriguez, M. Blanchot, C. Linder and B. Zimmermann, *Pure Appl. Chem.*, 2008, **80**, 1725–1733; (*b*) L. J. Gooßen, N. Rodriguez and K. Gooßen, *Angew. Chem., Int. Ed.*, 2008, **47**, 3100–3120.
4 (*a*) L. Yin, M. Kanai and M. Shibasaki, *J. Am. Chem. Soc.*, 2009, **131**, 9610–9611; (*b*) P. F. Lu, C. Sanchez, J. Cornella and I. Larrosa, *Org. Lett.*, 2009, **11**, 5710–5713; (*c*) L. J. Goossen, C. Linder, N. Rodriguez, P. P. Lange and A. Fromm, *Chem. Commun.*, 2009, 7173–7175; (*d*) R. Shang, Y. Fu, Y. Wang, Q. Xu, H. Z. Yu and L. Liu, *Angew. Chem., Int. Ed.*, 2009, **48**, 9350–9354.
5 (*a*) M. Nilsson, *Acta Chem. Scand.*, 1966, **20**, 423–426; (*b*) L. J. Gooßen, G. Deng and L. M. Levy, *Science*, 2006, **313**, 662–664.
6 J. Roithová and D. Schröder, *Coord. Chem. Rev.*, 2009, **253**, 666–677.
7 R. A. J. O'Hair, in *MS investigations of reactive intermediates in solution*, ed. L. S. Santos, Wiley-VCH, Weinheim, 2010, ch. 6, pp. 199–227.
8 (*a*) R. A. J. O'Hair, *Chem. Commun.*, 2002, 20–21; (*b*) P. F. James and R. A. J. O'Hair, *Org. Lett.*, 2004, **6**, 2761–2764; (*c*) N. Rijs, T. Waters, G. N. Khairallah and R. A. J. O'Hair, *J. Am. Chem. Soc.*, 2008, **130**, 1069; (*d*) N. J. Rijs and R. A. J. O'Hair, *Organometallics*, 2009, **28**, 2684–2692; (*e*) N. J. Rijs, B. F. Yates and R. A. J. O'Hair, *Chem.–Eur. J.*, 2010, **16**, 2674–2678; (*f*) N. J. Rijs and R. A. J. O'Hair, *Organometallics*, 2010, **29**, 2282–2291.
9 (*a*) M. T. Reetz, *Adv. Organomet. Chem.*, 1977, **16**, 33–65; (*b*) I. Fernandez, F. P. Cossio and M. A. Sierra, *Chem. Rev. (Washington, DC, U. S.)*, 2009, **109**, 6687–6711; (*c*) I. D. Gridnev, *Coord. Chem. Rev.*, 2008, **252**, 1798–1818.
10 (*a*) A. Tamaki and J. K. Kochi, *J. Organomet. Chem.*, 1973, **51**, C39–C42; (*b*) G. W. Rice and R. S. Tobias, *Inorg. Chem. (Washington, DC, U. S.)*, 1975, **14**, 2402–2407; (*c*) G. W. Rice and R. S. Tobias, *Inorg. Chem. (Washington, DC, U. S.)*, 1976, **15**, 489–490.
11 D. Zhu, S. V. Lindeman and J. K. Kochi, *Organometallics*, 1999, **18**, 2241–2248.
12 (*a*) A. Tamaki and J. K. Kochi, *J. Chem. Soc., Dalton Trans.*, 1973, 2620–2626; (*b*) S. Komiya, T. A. Albright, R. Hoffmann and J. K. Kochi, *J. Am. Chem. Soc.*, 1976, **98**, 7255–7265; (*c*) S. Komiya, T. A. Albright, R. Hoffmann and J. K. Kochi, *J. Am. Chem. Soc.*, 1977, **99**, 8440–8447; (*d*) G. Hallnemo and C. Ullenius, *Tetrahedron*, 1983, **39**, 1621–1625; (*e*) O. Schuster and H. Schmidbaur, *Inorg. Chim. Acta*, 2006, **359**, 3769–3775.
13 (*a*) P. Schwerdtfeger, *J. Am. Chem. Soc.*, 1990, **112**, 2818–2820; (*b*) J. A. Tossell, *Chem. Phys. Lett.*, 1998, **286**, 73–78; (*c*) W. Nakanishi, M. Yamanaka and E. Nakamura, *J. Am. Chem. Soc.*, 2005, **127**, 1446–1453; (*d*) P. Schwerdtfeger, H. L. Hermann and H. Schmidbaur, *Inorg. Chem.*, 2003, **42**, 1334–1342.
14 A. K. Chowdhury and C. L. Wilkins, *J. Am. Chem. Soc.*, 1987, **109**, 5336–5343.
15 (*a*) R. J. Puddephatt, in *Comprehensive Organometallic Chemistry*, ed. G. Wilkinson, F. G. A. Stone and E. W. Abel, Pergamon, Oxford, 1982, vol. 2, pp. 765–821; (*b*) A. Grohmann and H. Schmidbaur, in *Comprehensive Organometallic Chemistry II*, ed. E. W. Abel, F. G. A. Stone

and G. Wilkinson, Elsevier, Oxford, 1995, vol. 3, pp. 1–56; (*c*) H. Schmidbaur and A. Schier, in *Comprehensive Organometallic Chemistry III*, ed. R. H. Crabtree and D. M. P. Mingos, Elsevier, Oxford, 2007, vol. 2, pp. 251–307; (*d*) R. V. Parish, *Gold Bull. (Geneva)*, 1997, **30**, 3–12; (*e*) R. V. Parish, *Gold Bull. (Geneva)*, 1997, **30**, 55–62; (*f*) R. V. Parish, *Gold Bull. (Geneva)*, 1998, **31**, 14–21.
16 L. Feketeová, G. N. Khairallah and R. A. J. O'Hair, *Eur. J. Mass Spectrom.*, 2008, **14**, 107–110.
17 (*a*) G. E. Reid, R. A. J. O'Hair, M. L. Styles, W. D. McFadyen and R. J. Simpson, *Rapid Commun. Mass Spectrom.*, 1998, **12**, 1701–1708; (*b*) T. Waters, R. A. J. O'Hair and A. G. Wedd, *J. Am. Chem. Soc.*, 2003, **125**, 3384–3396.
18 (*a*) P. Pyykko, *Angew. Chem., Int. Ed.*, 2004, **43**, 4412–4456; (*b*) P. Pyykko, *Inorg. Chim. Acta*, 2005, **358**, 4113–4130; (*c*) P. Pyykko, *Chem. Soc. Rev.*, 2008, **37**, 1967–1997.
19 *Gaussian_03*. M. J. Frisch, *et al.*, Gaussian, Inc., Pittsburgh PA, 2003.
20 (*a*) A. D. Becke, *J. Chem. Phys.*, 1993, **98**, 5648–5652; (*b*) C. Lee, W. Yang and R. G. Parr, *Phys. Rev. B: Condens. Matter*, 1988, **37**, 785–789.
21 (*a*) M. Dolg, U. Wedig, H. Stoll and H. Preuss, *J. Chem. Phys.*, 1987, **86**, 866–872; (*b*) P. C. Hariharan and J. A. Pople, *Theor. Chim. Acta*, 1973, **28**, 213–222; (*c*) T. Clark, J. Chandrasekhar and P. V. R. Schleyer, *J. Comput. Chem.*, 1983, **4**, 294–301; (*d*) R. Krishnam, J. S. Binkley, R. Seeger and J. A. Pople, *J. Chem. Phys.*, 1980, **72**, 650–654; (*e*) P. M. W. Gill, B. G. Johnson, J. A. Pople and M. J. Frisch, *Chem. Phys. Lett.*, 1992, **197**, 499–505.
22 X. J. Liu, C. L. Yang, X. Zhang, K. L. Han and Z. C. Tang, *J. Comput. Chem.*, 2008, **29**, 1667–1674.
23 (*a*) G. N. Khairallah, R. A. J. O'Hair and M. I. Bruce, *Dalton Trans.*, 2006, 3699; (*b*) S. Buckart, G. Gantefoer, Y. D. Kim and P. Jena, *J. Am. Chem. Soc.*, 2003, **125**, 14205; (*c*) L. Andrews, *Chem. Soc. Rev.*, 2004, **33**, 123.
24 Y. Feng, L. Liu, J. T. Wang, H. Huang and Q. X. Guo, *J. Chem. Inf. Model.*, 2003, **43**, 2005–2013.
25 L. M. Pratt, S. Voit, B. K. Mai and B. H. Nguyen, *J. Phys. Chem. A*, 2010, **114**, 5005–5015.
26 S. Gronert, *J. Am. Soc. Mass Spectrom.*, 1998, **9**, 845.
27 M. A. Carvajal, J. J. Novoa and S. Alvarez, *J. Am. Chem. Soc.*, 2004, **126**, 1465–1477.

